

## Article

# Evaluation of Post-Stroke Impairment in Fine Tactile Sensation by Electroencephalography (EEG)-Based Machine Learning

Jianing Zhang<sup>1</sup>, Yanhuan Huang<sup>1</sup>, Fuqiang Ye<sup>1</sup>, Bibo Yang<sup>1</sup>, Zengyong Li<sup>2</sup> and Xiaoling Hu<sup>1,3,4,5,\*</sup>

<sup>1</sup> Department of Biomedical Engineering, The Hong Kong Polytechnic University, Hong Kong 999077, China; jayce.zhang@connect.polyu.hk (J.Z.); yanhuan.huang@connect.polyu.hk (Y.H.); 19073922r@connect.polyu.hk (F.Y.); bibo.yang@polyu.edu.hk (B.Y.)

<sup>2</sup> National Research Centre for Rehabilitation Technical Aids Beijing, Beijing Key Laboratory of Rehabilitation Technical Aids for Old-Age Disability, Beijing 100176, China; lizengyong@nrcrta.cn

<sup>3</sup> University Research Facility in Behavioural and Systems Neuroscience (UBSN), The Hong Kong Polytechnic University, Hong Kong 999077, China

<sup>4</sup> Shenzhen Research Institute, The Hong Kong Polytechnic University, Shenzhen 518000, China

<sup>5</sup> Research Institute for Smart Ageing (RISA), The Hong Kong Polytechnic University, Hong Kong 999077, China

\* Correspondence: xiaoling.hu@polyu.edu.hk; Tel.: +852-3400-3206

**Abstract:** Electroencephalography (EEG)-based measurements of fine tactile sensation produce large amounts of data, with high costs for manual evaluation. In this study, an EEG-based machine-learning (ML) model with support vector machine (SVM) was established to automatically evaluate post-stroke impairments in fine tactile sensation. Stroke survivors ( $n = 12$ , stroke group) and unimpaired participants ( $n = 15$ , control group) received stimulations with cotton, nylon, and wool fabrics to the different upper limbs of a stroke participant and the dominant side of the control. The average and maximal values of relative spectral power (RSP) of EEG in the stimulations were used as the inputs to the SVM-ML model, which was first optimized for classification accuracies for different limb sides through hyperparameter selection ( $\gamma$ ,  $C$ ) in radial basis function (RBF) kernel and cross-validation during cotton stimulation. Model generalization was investigated by comparing accuracies during stimulations with different fabrics to different limbs. The highest accuracies were achieved with ( $\gamma = 2^1$ ,  $C = 2^3$ ) for the RBF kernel (76.8%) and six-fold cross-validation (75.4%), respectively, in the gamma band for cotton stimulation; these were selected as optimal parameters for the SVM-ML model. In model generalization, significant differences in the post-stroke fabric stimulation accuracies were shifted to higher (beta/gamma) bands. The EEG-based SVM-ML model generated results similar to manual evaluation of cortical responses to fabric stimulations; this may aid automatic assessments of post-stroke fine tactile sensations.

**Keywords:** stroke; fine tactile sensation; electroencephalography; machine learning; evaluation



**Citation:** Zhang, J.; Huang, Y.; Ye, F.; Yang, B.; Li, Z.; Hu, X. Evaluation of Post-Stroke Impairment in Fine Tactile Sensation by Electroencephalography (EEG)-Based Machine Learning. *Appl. Sci.* **2022**, *12*, 4796. <https://doi.org/10.3390/app12094796>

Academic Editors: Leonardo Rundo, Carmelo Militello and Andrea Tangherloni

Received: 25 March 2022

Accepted: 6 May 2022

Published: 9 May 2022

**Publisher's Note:** MDPI stays neutral with regard to jurisdictional claims in published maps and institutional affiliations.



**Copyright:** © 2022 by the authors. Licensee MDPI, Basel, Switzerland. This article is an open access article distributed under the terms and conditions of the Creative Commons Attribution (CC BY) license (<https://creativecommons.org/licenses/by/4.0/>).

## 1. Introduction

Approximately 50% of stroke survivors have reported persistent sensory deficiencies for both somatosensation and proprioception [1,2]. For example, they often have difficulties in perceiving pain, temperature, pressure, posture, and light touch [3]. Sensory deficiencies have profound negative impacts on the functional ability and independency in daily living, which further affect motor recovery after stroke [4,5]. Fine tactile sensation is an elementary somatosensory function for obtaining external information through touch [6]. Previous studies have shown that fine tactile sensation also provide valid spatial references for body positions to reduce postural sway [7], and it may act as an indicator to enhance sensory feedback in position control [8,9]. However, rehabilitation for sensory functions has been overlooked in the traditional practices, when compared with efforts for motor restoration; this is attributed to the lack of effective evaluation measures for sensory impairments [10].

Objective and efficient assessments of sensory impairments are important for long-term post-stroke rehabilitation with repeated measurements during follow up [11]. However, subjective and manual measurements have been used traditionally for sensory impairment assessments [12]. For example, the Fugl–Meyer assessment (FMA) [13] and Semmes–Weinstein monofilament test [14] are commonly used in current evaluations of fine tactile sensations because of the ease of interpretation of the assessment results. Additionally, the measurement process highly relies on the personal experiences of the assessor, where achieving consistency in measurements is challenging when the stroke population increases during long-term service [15].

Neuroimaging techniques have been introduced to provide objective data for sensory impairment assessments [16]. The common neuroimaging techniques include functional magnetic resonance imaging (fMRI), positron emission tomography (PET), neuromolecular imaging, and electroencephalography (EEG), among others [17–23]. These approaches characterize neural circuitry changes during post-stroke sensorimotor recovery; however, such medical equipment is expensive and the preparations before neuroimaging-based examinations are complicated compared to the traditional clinical assessments [24]. Among these techniques, owing to the advantage of high temporal resolution, EEG has been applied to detect transient sensory neural responses during fine tactile stimulations [25,26]. For example, Ahn et al. compared the effects of different tactile exploration tasks, i.e., passively or actively moving a tactile board, on post-stroke brain activation using EEG [27]. The sensory motor rhythm indicated by the EEG relative powers from the right prefrontal and parietal lobes during active tactile perceptions were significantly greater than those in the damaged left hemisphere during passive tactile perception [27]. In our previous work [28], post-stroke sensory impairment of fine tactile sensation was measured quantitatively via EEG during textile fabric stimulation, i.e., simulation of the common fabric–skin touch. We observed EEG relative spectral power (RSP) differences after stroke, i.e., RSP intensities in different frequency bands between unimpaired and stroke populations [28]. However, neuroimaging-based measurements usually generate large amounts of data, whose interpretations still heavily rely on human professionals, which is time consuming and labor demanding [29,30].

Neuroimaging data interpretation by machine-learning (ML) techniques has been a promising approach to reduce manpower workload in data interpretations [31]. ML is a technique that can help develop an automatic predictive model by learning the relationships between features and targets from a given set of historical data before application to repeated analyses on massive data [32]. Various ML algorithms, e.g., linear discriminant analysis (LDA), artificial neural network (ANN), and support vector machine (SVM), are being explored for the detection, classification, and characterization of neuroimaging data, e.g., EEG [31]. For instance, Jochumsen et al. classified single-trial movement intentions associated with different hand grasp types using the EEG spectra as input features to an LDA model [33]. Usama et al. distinguished correct/error feedbacks during hand and foot movements by feeding the EEG waveform features into an ANN model [34]. Limited classification accuracies were obtained in both studies: 41–86% [33,34]. This may be attributed to insufficiencies in feature mapping by simple linear transformation of the LDA, leading to inefficient construction of the optimal decision function (classification boundary) for multichannel EEG [35,36]. Although ANN-based models offer nonlinear feature mapping abilities during classifications, overfitting often occurs when there are several hyperparameters, e.g., numbers of hidden layers and nodes, to be determined during network optimization [36]. In contrast to the ANN, SVM-based models reduce the disadvantages of overfitting of the classification results with the help of kernel functions [37]. SVM with kernel functions effectively minimize model complexities via implicitly realizing nonlinear transformations of the feature spaces without explicit mathematical expressions, so that only specific hyperparameters related to the kernel functions of the SVM need to be optimized during model development [38]. In the SVM-ML models, several kernel functions are commonly used, namely linear, polynomial, and radial basis function (RBF)

kernels. For example, Liu et al. extracted the spectrum features from subject-related EEG frequency bands and channels, and the SVM with linear kernel was applied to each subject's EEG-based motor imagery classification [39]. Ghumman et al. investigated the classification performance of SVM with a polynomial kernel in multiclass motor imagery EEG [40]. Bousseta et al. used SVM with RBF kernel to classify the EEGs of imagined hand movements [41]. These studies reported a classification range of 67–92.8% [39–41]. Among the practical applications of the kernel functions mentioned above, the RBF kernel is a common choice in SVM-ML models because of its better performance on the nonlinearities in feature mapping capabilities with less hyperparameters compared to the other two types of kernel functions [42,43].

Automatic evaluations of neuroimaging data by SVM-ML techniques have not been fully explored in literature, e.g., fine tactile sensation. Kim et al. extracted the powers of the alpha and gamma bands as features representing EEG during touch with different objects, i.e., fabric, glass, and paper [44]. However, they only evaluated the tactile perception of unimpaired persons and obtained limited classification performance (68.1%) with the LDA model [44]. The purpose of this study was to automatically evaluate and assess post-stroke impairments in fine tactile sensation using a new EEG-based SVM-ML model.

## 2. Methodology

In this study, an SVM-ML model was established based on EEG measurements of cortical responses to fine tactile stimulations to the upper limbs in persons who have experienced stroke and in unimpaired participants via stimulations with different types of fabrics (cotton, nylon, and wool). The SVM-ML model was first developed and optimized using EEG RSP features with cotton fabric stimulation as the baseline input for classifying the responses from multiple upper limb groups, i.e., stimulation to the (1) affected sides of persons after stroke (SA), (2) unaffected sides of persons after stroke (SU), and (3) dominant sides of unimpaired participants (UD). Then, the generalization performance of the model was evaluated using the EEG RSP features during stimulations with different fabrics with and without considering arm differences.

### 2.1. EEG Acquisitions during Fabric Stimulations

After obtaining ethical approval from the Human Subjects Ethics Sub-committee (HSESC) of the Hong Kong Polytechnic University, twelve survivors of chronic stroke were recruited as the “stroke group”, and fifteen unimpaired participants were recruited as the “control group”, whose demographic details are listed in Table 1. The inclusion criteria of stroke group were: (1) individuals must be at least six months after the singular and unilateral brain lesion due to stroke; (2) the lesions occurring due to stroke were experienced in the subcortical area, to ensure the detectable EEG from the cortical area. All unimpaired participants were right-handed. No significant difference was found in age between the stroke and control groups ( $p > 0.05$ ) by the independent  $t$ -test after verifying normality evaluations via the Shapiro–Wilk test [45].

**Table 1.** Demographic characteristics and clinical scores of the stroke and control groups [28].

Measure	Stroke Group ( $n = 12$ )	Control Group ( $n = 15$ )
Age in years	55.1 ± 16.0	46.4 ± 17.4
Gender (male/female)	11/1	5/10
Stroke type (ischemic/hemorrhagic)	10/2	-
Affected side (right/left)	6/6	-
Years since stroke	14.9 ± 5.8	-
FMA (upper extremity)	42.5 ± 15.2	-
FMA (light touch on forearm)	1 ± 0	-
MAS (elbow)	1.1 ± 0.7	-

Note: Data are given as mean ± standard deviation. MAS: Modified Ashworth scale; FMA: Fugl–Meyer assessment [28].

The experimental setup and protocol for the fabric fine tactile stimulation are shown in Figure 1. The three types of fabrics, i.e., cotton, nylon, and wool of the same size and different textural properties, were alternatively placed on the skin surface of the ventral forearm of the upper limb, i.e., a single stimulation trial (Figure 1c). Each trial consisted of a 30 s baseline measurement, i.e., no fabric stimulation to the skin, followed by alternative stimuli with the three different fabrics in a random sequence for 13 s stimulation with each fabric and 60 s gaps in between. The stimulation trial was repeated thrice for each target forearm. The whole brain EEG with 64 channels (BP-01830, Brain Products Inc., Gilching, Germany) based on the 10–20 system [46] was captured during the stimulation trials at a sampling frequency of 1000 Hz. Each subject was required to stay awake and calm during the EEG measurements while wearing ear plugs and an eye mask, whose purpose was to minimize visual and audio disturbances from the environment. The detailed experimental procedure is described in [28].

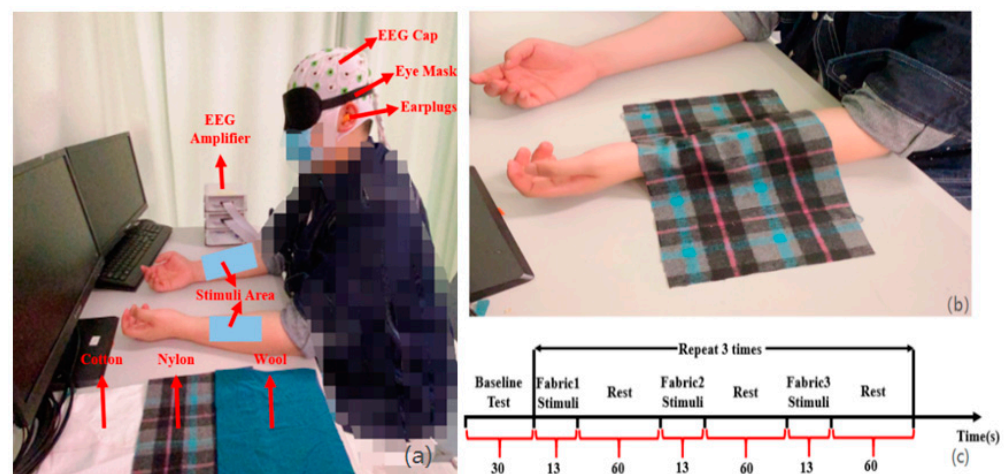


**Figure 1.** Electroencephalography (EEG) experimental setup and protocol. (a) Participant wearing the EEG cap, ear plugs, and eye mask, is seated in a chair and tested with their hands comfortably placed on the table. The areas of each fabric stimulation are the ventral forearms. The three fabric samples, namely cotton, nylon, and wool, are placed on the table. (b) Illustration of fabric stimulation. The nylon fabric is placed on the ventral forearm. (c) Protocol for fabric stimulation.

## 2.2. EEG-Specific Feature Extraction for the SVM-ML Model

In this work, the  $RSP_{\text{mean}}$  and  $RSP_{\text{max}}$  values in different frequency bands were selected as the EEG features for input to the SVM-ML model as they represent the average and maximal cortical changes, respectively, during fabric stimulations based on manual recognition from the previous study [28]. During the real-time EEG recording, the sampling frequency was 1000 Hz. In the preparation of the EEG RSP features, a Butterworth bandpass filter from 0.1 to 100 Hz was first applied to the EEG to eliminate irrelevant high-frequency components. Then, an additional Butterworth notch filter from 49 Hz to 51 Hz was applied to eliminate the 50 Hz noise from the environment. Following this, the filtered EEG was segmented into different epochs, i.e., 30 s pre-stimulus baseline and three 13 s stimuli with different fabrics. The numbers of EEG samples after segmentation were 108 from the SA group (12 participants  $\times$  3 trials  $\times$  3 fabric stimuli), 108 for the SU group (12 participants  $\times$  3 trials  $\times$  3 fabric stimuli), and 135 for the UD group (15 participants  $\times$  3 trials  $\times$  3 fabric stimuli). Next, the EEG samples were transformed into their power spectra by Pwelch estimation [47], and the entire frequency band (0.1–100 Hz) of each segmented EEG epoch was decomposed into five frequency bands, i.e., delta (0.5–4 Hz), theta (4–8 Hz), alpha

(8–12 Hz), beta (12–30 Hz), and gamma (30–100 Hz) [48]. Finally, the RSP [49] of each frequency band for each fabric stimulus was calculated using the following equations:

$$P(f_1, f_2) = \int_{f_1}^{f_2} p(f)df \quad (1)$$

$$RSP(f_1, f_2) = \frac{P(f_1, f_2)}{P(0.1, 100)} - \frac{P_{\text{baseline}}(f_1, f_2)}{P(0.1, 100)}, \quad (2)$$

where  $p(f)$  is the power spectral density;  $f_1$  and  $f_2$  are the low and high cutoff frequencies of a given EEG frequency band, respectively;  $P(f_1, f_2)$  is the power spectrum from  $f_1$  to  $f_2$ ; and  $P_{\text{baseline}}$  is the power spectrum of the EEG segments during the baseline test in each trial. The above spectral analysis of the raw EEG signals was implemented offline with the EEGLAB v12 toolbox in MATLAB (The MathWorks Inc., Natick, MA, USA).

After obtaining the RSP value from each EEG channel, the  $RSP_{\text{mean}}$  and  $RSP_{\text{max}}$  values were acquired to represent the RSP features of the multichannel EEG, where  $RSP_{\text{mean}}$  is the average value of the RSPs of all the channels in a given frequency band of a signal epoch, and  $RSP_{\text{max}}$  is the highest value among all the EEG channels. Then, the  $RSP_{\text{mean}}$  and  $RSP_{\text{max}}$  of the 62-channel EEG (ground and reference channels were neglected), which covered the entire cortical area, were calculated for each frequency band. To minimize the diversity of the ranges for the  $RSP_{\text{mean}}$  and  $RSP_{\text{max}}$ , the original  $RSP_{\text{mean}}$  and  $RSP_{\text{max}}$  were further normalized as in the following equation according to z-score normalization, which scales all the  $RSP_{\text{mean}}$  and  $RSP_{\text{max}}$  values in varying ranges with a zero mean and unit standard deviation [50]:

$$RSP_i' = \frac{RSP_i - \mu_{RSP}}{\sigma_{RSP}}, \quad (3)$$

where  $RSP_i$  is the original spectral feature, i.e.,  $RSP_{\text{mean}}$  or  $RSP_{\text{max}}$ ;  $\mu_{RSP}$  is the mean of  $RSP_i$ ;  $\sigma_{RSP}$  is the standard deviation of  $RSP_i$ ; and  $RSP_i'$  is the normalized spectral feature. The normalized features were then used as the inputs to the SVM-ML model.

### 2.3. SVM-ML Model Configuration

Figure 2 shows the configuration of the SVM-ML model, including optimization of the SVM RBF kernel function and k-fold cross-validation (CV) strategy. The normalized EEG features (i.e.,  $RSP_{\text{mean}}$  and  $RSP_{\text{max}}$ ) during stimulation with cotton fabric were adopted as the baseline inputs for model establishment. This is because cotton is the most widely used fabric that is in intimate contact with skin in daily living and provides minimum stimulation intensity with a comfortable feeling compared to other fabrics [51]. In addition, compared to nylon and wool, the textile physical properties of cotton fabric as quantitatively measured by the fabric touch tester (FTT) [52] were neutral with equivalent distances in the aspects of smoothness, thickness, etc. [28]. Therefore, the EEG RSP features evoked by the cotton fabric were used as the baseline inputs to configure the SVM-ML model.

The RBF kernel function of the SVM-ML model was determined by optimizing the classification boundaries that achieved the best accuracy on the RSP features related to cotton stimulation. For an RBF kernel, two hyperparameters, namely the kernel scaling parameter  $\gamma$  and regularization parameter  $C$  [53], are optimized in the SVM-ML model development to classify the different upper-limb groups. The search for optimal  $(\gamma, C)$  was conducted by a “grid search” approach [54]. The candidate values of  $(\gamma, C)$  were first defined as exponentially increasing sequences ( $\gamma = 2^{-15}, 2^{-13}, \dots, 2^9$ ;  $C = 2^{-5}, 2^{-3}, \dots, 2^{15}$ ), which were the ranges adopted by most EEG-based SVM-ML studies to identify the optimal  $(\gamma, C)$  values [42,55,56]. Following this, different pairs of  $\gamma$  and  $C$  ( $13 \times 11 = 143$  pairs) values were generated, and each pair was used to construct the RBF kernel of the SVM. The classification accuracies with the different hyperparameter pairs were evaluated by three-fold CV according to the greatest common divisor of the number of stroke patients (i.e.,  $n = 12$ ) and unimpaired controls (i.e.,  $n = 15$ ); this is a common pilot estimation approach used in previous studies [57]. The value pair that achieved the best classification

accuracy was then adopted as the optimal hyperparameters for model configuration. The above SVM algorithm was implemented using the Scikit-learn toolbox, an open-source ML toolbox in Python [58].

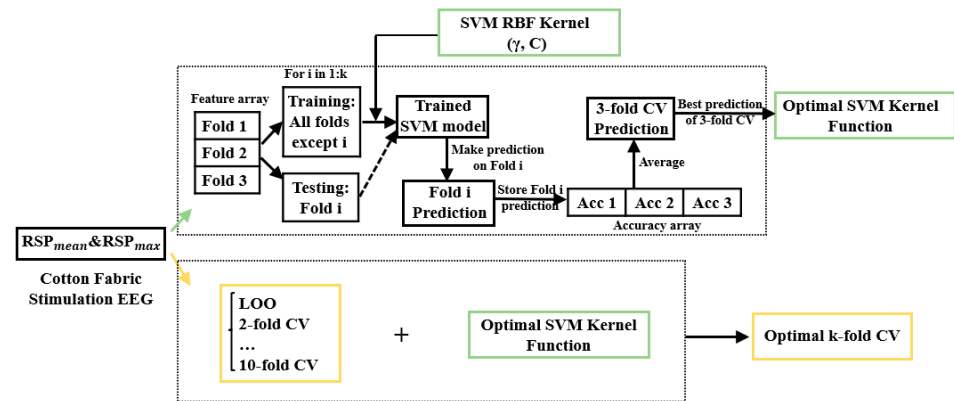


**Figure 2.** Configuration flowchart for the SVM-ML model. RSP: relative spectral power; SVM: support vector machine; RBF: radial basis function; Acc: accuracy; LOO: leave-one-out; CV: cross validation.

The grid search results of  $\gamma$  and  $C$  are displayed in Figure 3, where Figure 3a–e present the accuracies of different  $(\gamma, C)$  pairs for distinguishing the UD, SA, and SU groups with the  $RSP_{\text{mean}}$  and  $RSP_{\text{max}}$  of the 62-channel EEG in the delta, theta, alpha, beta, and gamma bands, respectively, as input features. The coordinates and values of the highest accuracy for each frequency band are indicated by the red dots in Figure 3a–e. Among all the accuracies, the model with the highest accuracy of 67.4% ( $\gamma = 2^3, C = 2^9$ ) was achieved in the gamma band.

As the sensorimotor cortex is the main response area for sensory stimulations [59], the classification performance achieved by including only the EEG channels covering the sensorimotor cortex was evaluated in the SVM-ML model configuration. The  $RSP_{\text{mean}}$  and  $RSP_{\text{max}}$  of the corresponding 21-channel EEG (i.e., FC1–FC6, FCZ, C1–C6, CZ, CP1–CP6, CPZ), which cover the sensorimotor area [60], were used as the inputs to the model. Figure 4 shows the accuracies with the RSP features for the 21-channel EEG, and the highest accuracy of 76.8% ( $\gamma = 2^1, C = 2^3$ ) was obtained for the gamma band as well.

The accuracies of the SVM-ML model for classifying the UD, SA, and SU groups with the RBF kernel hyperparameter pairs in the different bands are summarized in Table 2. Compared to other frequency bands, the gamma band has the best average accuracy performance for both channel set selections. The average and peak accuracies of the gamma band of the 21-channel EEG were better than those of the 62-channel EEG. Therefore, the hyperparameter pair ( $\gamma = 2^1, C = 2^3$ ) from the 21-channel EEG was selected as the optimal RBF kernel hyperparameters.

After the RBF kernel function was determined, the  $k$ -fold CV was also configured using the RSP features of the 21-channel EEG as inputs to improve generalization of the SVM-ML model. Compared to the simple train/test split, the  $k$ -fold CV ensures that each sample from the original dataset has the chance of appearing in the training and testing set, which results in less biased evaluations [61]. Since the partition of  $k$  folds is random, the  $k$ -fold CV was performed 10 times to calculate the mean estimate to decrease the variance of accuracy estimations of the one-shot  $k$ -fold CV [62–64]. Typically, the configuration of  $k$  is 5 or 10, as these values have been shown to be the bias-variance trade-off for model evaluation [61,65]. In our experiment, different selections of  $k$  from 2 to 10 were employed to compare the influence of  $k$  on model performance. In addition, the leave-one-out CV, where  $k$  is the number of samples in the dataset, was used as a complementary comparison to different  $k$ -fold CV. Although the leave-one-out CV is more computationally expensive compared to the above strategies, i.e., five-fold and ten-fold CV, it offers an unbiased

evaluation of the model performance as each sample is given the opportunity to represent the entirety of the test dataset [61].

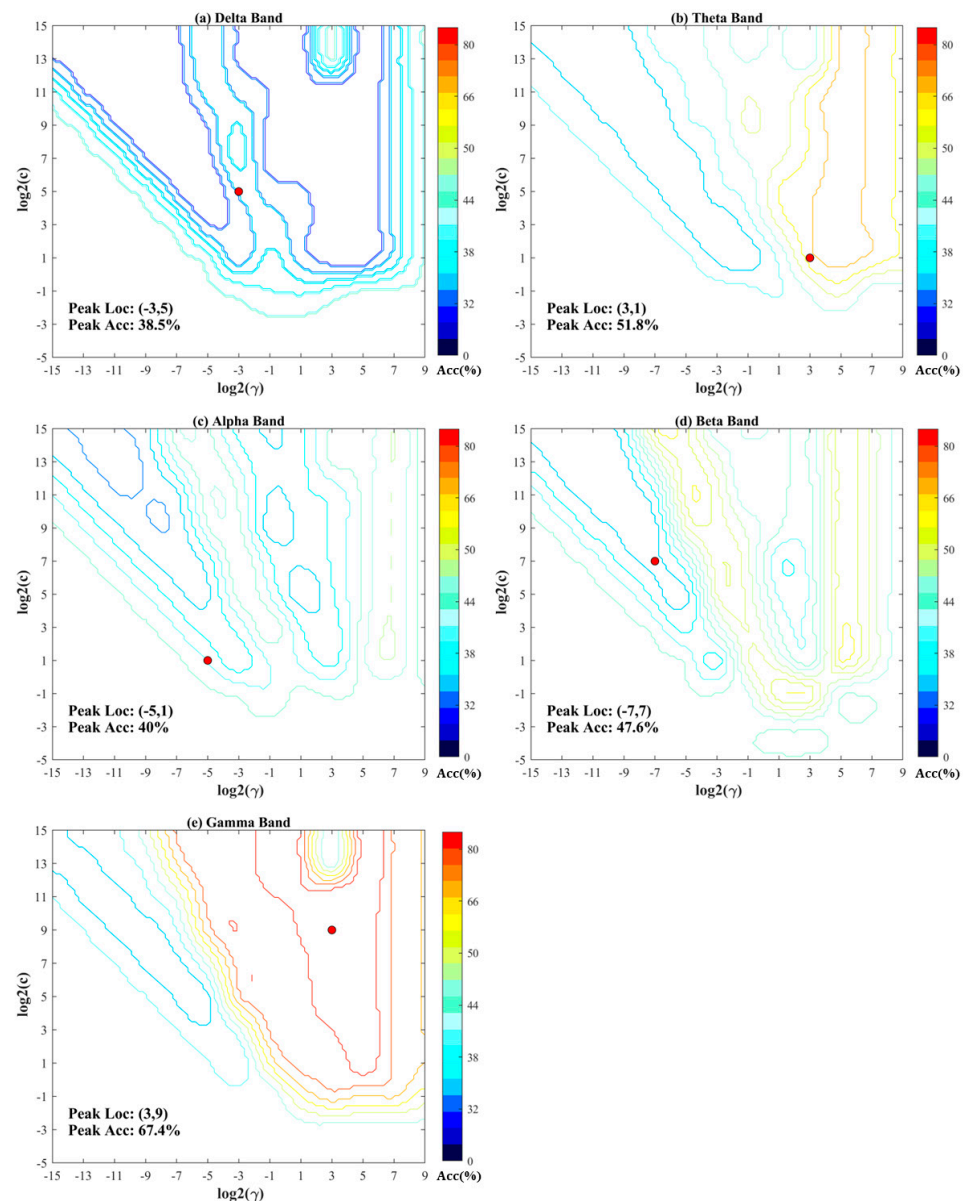


**Figure 3.** Grid search results of  $\gamma$  and  $C$  in the SVM-ML model with RBF kernel using the 62-channel EEG RSP features of the delta, theta, alpha, beta, and gamma bands. Acc: accuracy. Peak Acc: highest classification accuracy of the SVM-ML model in the predefined range of ( $\gamma, C$ ); Peak Loc: location ( $\gamma, C$ ) corresponding to the highest classification accuracy of the SVM-ML model.

The accuracies of the SVM-ML model for distinguishing between the UD, SA, and SU groups with different k-fold CV strategies in the different frequency bands are shown in Table 3. The model achieved the highest accuracy of 75.4% in the gamma band by six-fold CV. For the leave-one-out CV, the model obtained the highest classification accuracy of 74.4% in the gamma band as well. Therefore, the six-fold CV was selected as the optimal evaluation strategy for the model when using the RSP features of the 21-channel EEG as inputs.

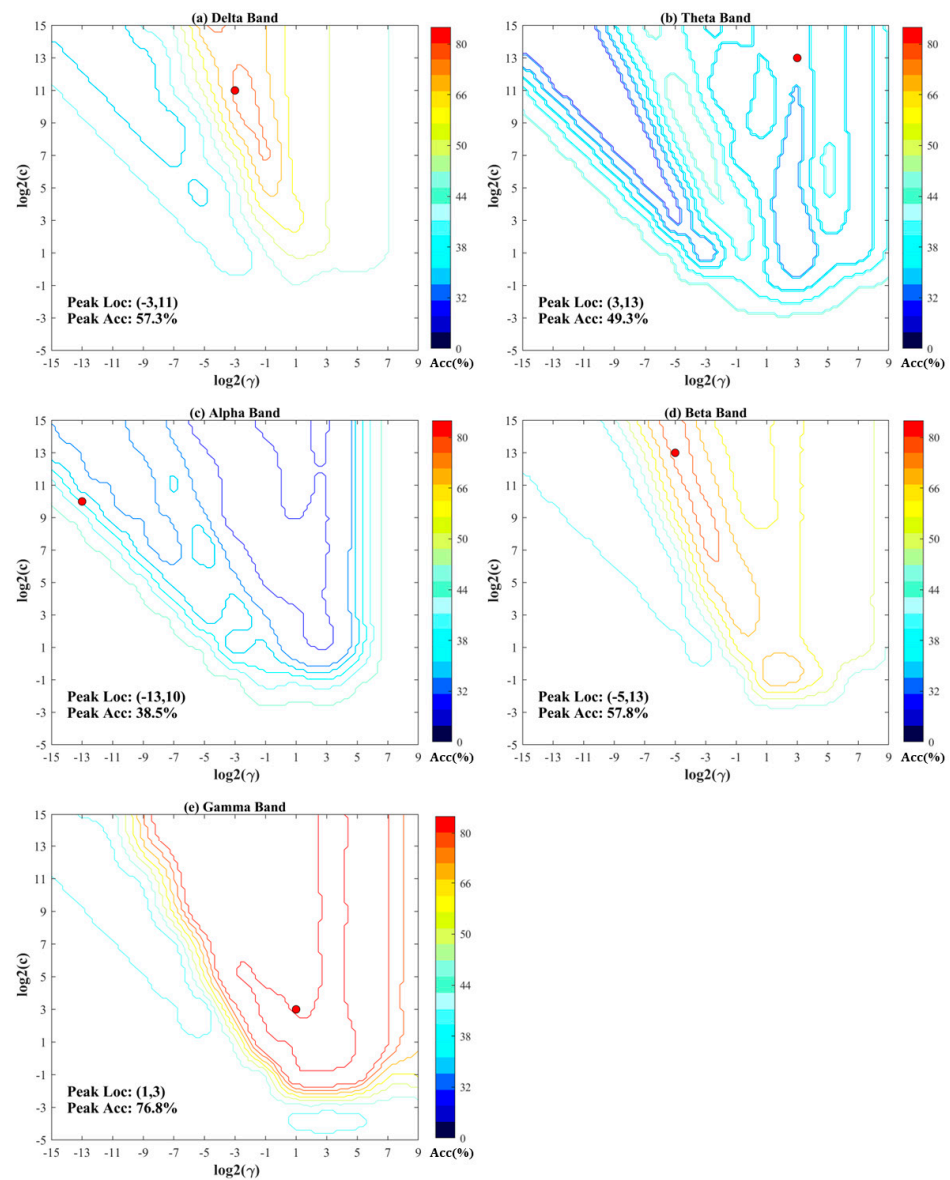


**Figure 4.** Grid search results of  $\gamma$  and  $C$  in the SVM-ML model with RBF kernel using the 21-channel EEG RSP features of the delta, theta, alpha, beta, and gamma bands. Acc: accuracy. Peak Acc: highest classification accuracy of the SVM-ML model in the predefined range of  $(\gamma, C)$ ; Peak Loc: location  $(\gamma, C)$  corresponding to the highest classification accuracy of the SVM-ML model.

#### 2.4. Generalization of the SVM-ML Model

Using the RSP features during stimulation with cotton fabric as the baseline inputs, the SVM-ML model was established. Then, we first investigated the generalization performance of the model for classifying the upper-limb groups with the inputs of different fabrics, i.e., nylon, wool, and cotton. The measured RSP features in the respective stimulations were then input to the developed model, and the achieved accuracies are summarized in Table 4. The classification accuracies of the different fabric stimulations were not normally distributed ( $p < 0.5$ , Shapiro–Wilk test) in each frequency band. Significant intergroup differences in the accuracies ( $p < 0.001$ , Kruskal–Wallis test) with respect to fabric stimulation were observed in the delta, theta, alpha, beta, and gamma bands. The model achieved the highest classification accuracies of 75.4%, 83.5%, and 84.3% for the cotton, nylon, and wool stimulations, respectively, in the gamma band.

**Table 2.** Accuracies of the SVM-ML model for classifying the three upper-limb groups with the RBF kernel hyperparameter pairs in different frequency bands.

Number of EEG Channels		Delta	Theta	Alpha	Beta	Gamma
62	Average Acc	33.5% ± 0.05	37.8% ± 0.05	35.8% ± 0.03	38.2% ± 0.04	44.7% ± 0.11
	Peak Acc	38.5%	51.8%	40.0%	47.6%	67.4%
	Peak Loc ( $\gamma, C$ )	( $2^{-3}, 2^5$ )	( $2^3, 2^1$ )	( $2^{-5}, 2^1$ )	( $2^{-7}, 2^7$ )	( $2^3, 2^9$ )
21	Average Acc	39.1% ± 0.06	35.6% ± 0.04	33.2% ± 0.06	41.3% ± 0.07	49.2% ± 0.16
	Peak Acc	57.3%	49.3%	38.5%	57.8%	76.8%
	Peak Loc ( $\gamma, C$ )	( $2^{-3}, 2^{11}$ )	( $2^3, 2^{13}$ )	( $2^{-13}, 2^{10}$ )	( $2^{-5}, 2^{13}$ )	( $2^1, 2^3$ )

Note: Average Acc: average classification accuracy of the SVM-ML model with all the RBF kernel hyperparameter pairs; Peak Acc: highest classification accuracy of the SVM-ML model in the predefined range of ( $\gamma, C$ ); Peak Loc: location ( $\gamma, C$ ) corresponding to the highest classification accuracy of the SVM-ML model.

**Table 3.** Accuracies of the SVM-ML model for classifying the three upper-limb groups with different k-fold CV strategies in the different frequency bands.

CV	Accuracy				
	Delta	Theta	Alpha	Beta	Gamma
2-fold	49.6% ± 0.07	38.1% ± 0.06	27.6% ± 0.06	50.7% ± 0.07	73.8% ± 0.05
3-fold	49.1% ± 0.06	33.3% ± 0.07	26.0% ± 0.05	51.0% ± 0.05	74.5% ± 0.04
4-fold	49.7% ± 0.06	34.7% ± 0.06	23.9% ± 0.05	50.1% ± 0.05	74.8% ± 0.04
5-fold	49.7% ± 0.06	32.4% ± 0.05	26.1% ± 0.05	51.2% ± 0.04	75.0% ± 0.03
6-fold	53.2% ± 0.05	35.0% ± 0.06	22.2% ± 0.05	50.8% ± 0.05	75.4% ± 0.04
7-fold	46.7% ± 0.06	32.6% ± 0.05	32.9% ± 0.05	48.2% ± 0.06	72.6% ± 0.04
8-fold	47.0% ± 0.07	31.3% ± 0.06	28.9% ± 0.06	47.2% ± 0.06	74.8% ± 0.04
9-fold	49.5% ± 0.07	31.4% ± 0.06	27.8% ± 0.06	49.1% ± 0.06	74.7% ± 0.05
10-fold	51.7% ± 0.07	33.0% ± 0.06	25.9% ± 0.06	50.0% ± 0.05	74.8% ± 0.05
LOO	51.3%	28.2%	12.8%	53.8%	74.4%

Note: Data are given as mean ± SD. CV: cross validation; LOO: leave-one-out.

**Table 4.** Overall accuracies of the SVM-ML model for classifying different fabric stimulations.

Fabric Stimulation	Accuracy				
	Delta	Theta	Alpha	Beta	Gamma
Cotton	53.2% ± 0.05	35.0% ± 0.06	22.3% ± 0.05	50.8% ± 0.05	75.4% ± 0.04
Nylon	21.0% ± 0.04	40.6% ± 0.05	51.4% ± 0.04	63.2% ± 0.03	83.5% ± 0.02
Wool	30.3% ± 0.04	25.6% ± 0.06	43.0% ± 0.05	69.2% ± 0.04	84.3% ± 0.03
Significance ( $p$ -value)	<0.001 ***	<0.001 ***	<0.001 ***	<0.001 ***	<0.001 ***

Note: Data are given as mean ± SD. The significant differences are indicated by '\*\*\*' ( $p < 0.001$ , Kruskal–Wallis test).

The comparison of the overall accuracies of the SVM-ML model with respect to fabric stimulation in each band are shown in Figure 5. Significant differences in the accuracies were observed in the delta, theta, alpha, beta, and gamma bands for pairwise comparisons among the three different fabric stimulations ( $p < 0.001$ , Kruskal–Wallis with Bonferroni post-hoc test), except for the difference between nylon and wool in the gamma band ( $p > 0.05$ , Kruskal–Wallis with Bonferroni post-hoc test). The models with nylon and wool achieved significantly higher accuracies in the beta and gamma bands than those with cotton ( $p < 0.001$ , Kruskal–Wallis with Bonferroni post-hoc test).

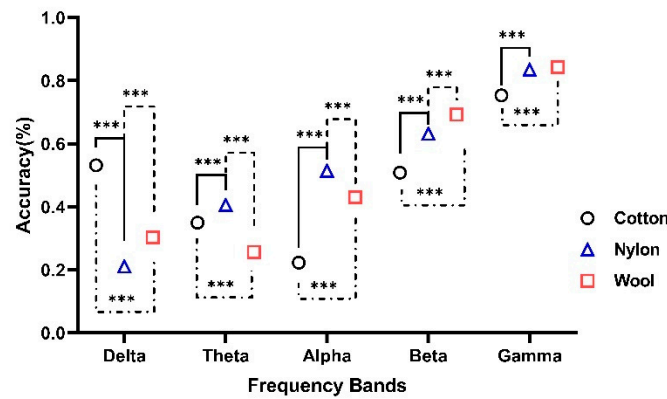


**Figure 5.** Comparisons of the overall classification accuracies of the SVM-ML model with respect to fabric stimulations in the delta, theta, alpha, beta, and gamma bands. The significant intergroup differences are indicated by ‘\*\*\*’ ( $p < 0.001$ , Kruskal–Wallis with Bonferroni post-hoc test).

The generalized performance of the model was also evaluated by considering the arm differences during stimulations with different fabrics (Table 5). The classification accuracies of each upper-limb group during stimulations with different fabrics are not normally distributed ( $p < 0.5$ , Shapiro–Wilk test). Significant differences in the accuracies ( $p < 0.001$ , Kruskal–Wallis test) with respect to fabric stimulations were observed in each band, except for the SU group in the gamma band ( $p > 0.05$ , Kruskal–Wallis test). The highest classification accuracy for each upper-limb group was achieved in the gamma band.

**Table 5.** Accuracies of the SVM-ML model for classifying the three upper-limb groups with different fabric stimulations.

Fabric Stimulation	Accuracy					
	Delta	Theta	Alpha	Beta	Gamma	
SA	Cotton	47.9% ± 0.09	28.8% ± 0.11	28.5% ± 0.10	48.9% ± 0.10	59.7% ± 0.08
	Nylon	26.8% ± 0.09	31.9% ± 0.08	54.1% ± 0.11	64.3% ± 0.10	76.2% ± 0.06
	Wool	22.9% ± 0.09	21.7% ± 0.08	51.1% ± 0.11	53.6% ± 0.08	78.9% ± 0.04
	<i>p</i> -value	<0.001 ***	<0.001 ***	<0.001 ***	<0.001 ***	<0.001 ***
SU	Cotton	48.3% ± 0.08	40.9% ± 0.13	27.0% ± 0.09	69.3% ± 0.05	91.0% ± 0.04
	Nylon	15.5% ± 0.07	40.5% ± 0.13	61.7% ± 0.04	74.9% ± 0.01	91.2% ± 0.03
	Wool	50.3% ± 0.03	27.8% ± 0.08	40.1% ± 0.04	84.9% ± 0.04	91.6% ± 0.01
	<i>p</i> -value	<0.001 ***	<0.001 ***	<0.001 ***	<0.001 ***	>0.05
UD	Cotton	51.4% ± 0.14	31.6% ± 0.10	22.0% ± 0.12	35.3% ± 0.12	78.0% ± 0.10
	Nylon	24.0% ± 0.09	51.9% ± 0.07	39.2% ± 0.10	53.7% ± 0.05	83.4% ± 0.01
	Wool	19.8% ± 0.09	30.0% ± 0.11	36.9% ± 0.10	71.9% ± 0.08	84.1% ± 0.06
	<i>p</i> -value	<0.001 ***	<0.001 ***	<0.001 ***	<0.001 ***	<0.001 ***

Note: Data are given as mean ± SD. The significant intergroup differences are indicated by ‘\*\*\*’ ( $p < 0.001$ , Kruskal–Wallis test).

Based on the results in Table 4 and Figure 5, the comparisons of the accuracies of the SVM-ML model with respect to fabric stimulations when considering arm differences are presented in Figure 6. In the SA group (Figure 6a), significant differences in accuracies with respect to the fabric stimulations were obtained in the higher frequency bands, i.e., beta ( $p < 0.001$ , Kruskal–Wallis with Bonferroni post-hoc test) and gamma ( $p < 0.05$ , Kruskal–Wallis with Bonferroni post-hoc test) bands. No significant differences were found between nylon and wool in the delta, theta, and alpha bands ( $p > 0.05$ , Kruskal–Wallis with Bonferroni post-hoc test). In the SU group (Figure 6b), significant differences in accuracies with

respect to fabric stimulations were found in the delta ( $p < 0.001$ , Kruskal–Wallis with Bonferroni post-hoc test), alpha ( $p < 0.001$ , Kruskal–Wallis with Bonferroni post-hoc test), and beta ( $p < 0.05$ , Kruskal–Wallis with Bonferroni post-hoc test) bands. No significant difference was observed between cotton and nylon in the theta band ( $p > 0.05$ , Kruskal–Wallis with Bonferroni post-hoc test). In the UD group (Figure 6c), significant differences in accuracies with respect to fabric stimulations were found in almost all frequency bands ( $p < 0.001$ , Kruskal–Wallis with Bonferroni post-hoc test), except for the difference between nylon and wool in the gamma band ( $p > 0.05$ , Kruskal–Wallis with Bonferroni post-hoc test).

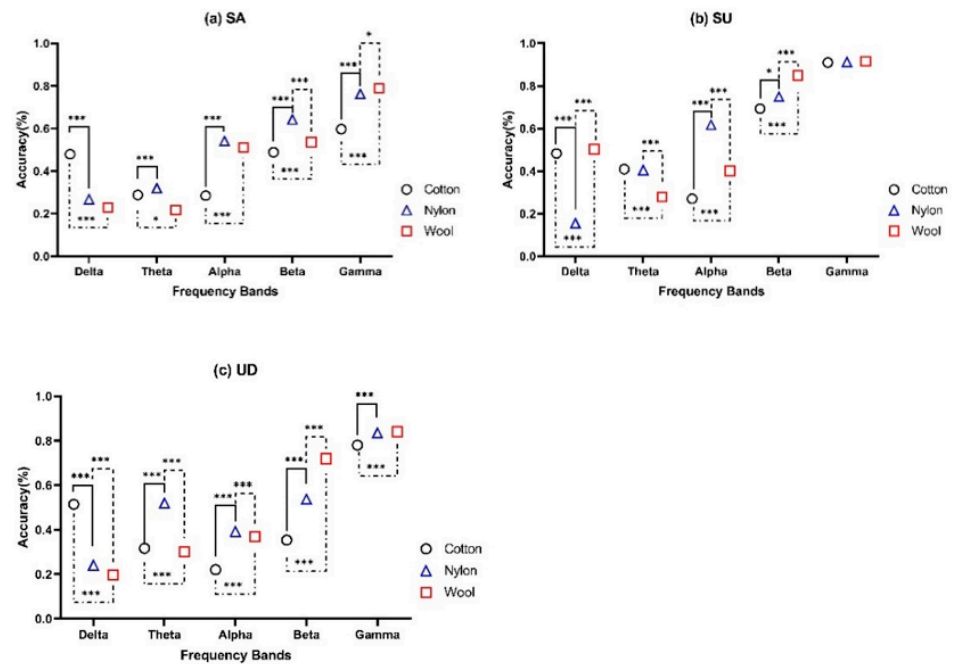


**Figure 6.** Comparisons of the classification accuracies of the SVM-ML model with respect to fabric stimulations when considering arm differences, i.e., (a) SA, (b) SU, and (c) UD. The significant differences are indicated by ‘\*’ for  $p < 0.05$  and ‘\*\*\*’ for  $p < 0.001$  (Kruskal–Wallis with Bonferroni post-hoc test).

### 3. Discussion

In this study, the EEG-based SVM-ML model was built using the RSP features during stimulation with cotton fabric as the baseline inputs. The model’s generalization performance was investigated by comparing the classification accuracies during stimulations with different fabrics.

#### 3.1. SVM-ML Configuration

##### 3.1.1. RBF Kernel Determination

The grid search results of the hyperparameter pair ( $\gamma$ ,  $C$ ) for the RBF kernel (Figures 3 and 4) showed that the highest classification accuracies were obtained in the predefined range of the hyperparameter pair. Similar boundaries of the hyperparameter pair ( $\gamma$ ,  $C$ ) were also applied in other SVM-based studies, e.g., Chang et al. used the boundaries of ( $e^{-8} \leq \gamma \leq e^8$ ,  $e^{-8} \leq C \leq e^8$ ) [66], and Hsu et al. selected the boundaries of ( $2^{-15} \leq \gamma \leq 2^3$ ,  $2^{-5} \leq C \leq 2^{15}$ ) [42]. This showed that the selected optimal hyperparameter pair ( $\gamma$ ,  $C$ ) was in the traditional search space, and the SVM-ML model with the general search space was feasible for classifying the RSP features extracted from EEG during sensory assessments. The kernel scaling parameter  $\gamma$  determines the complexity of the classification decision function of the model [67]. For smaller values of  $\gamma$ , the decision function is nearly linear, and for larger values of  $\gamma$ , the function becomes more curved [67]. The optimal value of  $\gamma$  ( $2^1$ ) chosen by the model was close to the upper boundary of the preset  $\gamma$  range, which

suggested that there was a relatively strong nonlinearity among the EEGs of multiple upper-limb groups in the original feature space, and the model obtained the “curved” decision function by mapping the raw EEG to a higher dimensional space. The regularization parameter  $C$  defines the penalty degree of the model for the percentage of deviation from the misclassified trained data [67]. As the value of  $C$  increases, its penalty degree for the model becomes larger, and the percentage of deviation of the misclassified data is smaller during the training phase. The optimal value of  $C$  ( $2^3$ ) selected by the model was relatively lower compared to the predefined range of  $C$ . This suggested that the model tolerated a greater percentage of misclassified training data when searching for the optimal decision function, indicating that there was an overlap among the different groups of EEG data points near the decision function. Meanwhile, the model with the optimal hyperparameter pair ( $\gamma$ ,  $C$ ) achieved an accuracy of 76.8%, which was comparable to those reported in studies on multiclass classification of EEG using SVM-ML models with accuracies exceeding 71.0% [68,69].

### 3.1.2. EEG Channel Selection

It was observed that the overall accuracies of the model with the 21-channel EEG were better than those of the 62-channel EEG when not considering arm differences (Table 2). The 21-channel EEG covers the sensorimotor cortex, which is the main response area to sensory stimulations [70,71]. The accuracies based on the 21-channel EEG suggested that direct cortical processing from the sensorimotor cortex was sufficient to capture the sensory differences generated by different fabric samples through the SVM-ML model. Previous studies have demonstrated that significant RSP variations for different EEG bands during sensory stimulations were mainly captured in the sensorimotor cortex for both unimpaired and stroke populations [28,72,73]. On the contrary, involuntary attention activities beyond the sensorimotor cortex were involved in passive fabric stimulation experiments [28]. This could be a hurdle to the recognition of cortical responses to fabric stimulations using the SVM-ML model. Meanwhile, voluntary cognitive activities were also found to disturb measurement of cortical responses to sensory stimulations [73,74]. For example, in post-stroke sensory evaluation by a subjective questionnaire, stroke persons with sensory impairments could distinguish different fabric stimulations because of the compensation of cognitive processing, e.g., individual experiences, to the residual sensory pathways [28]. In this work, the voluntary cognitive activities were minimized by asking the participants to stay awake but mentally inactive during the fabric stimulations. Therefore, the EEG RSP features of the sensorimotor cortex detected by the 21-channel EEG were sufficient for representing the differences in direct cortical responses to fine tactile sensations.

Table 2 also shows that when identifying different fabric stimulations without considering arm differences, the model achieved better overall accuracies in higher bands, i.e., the beta and gamma bands. This was consistent with the results of previous neurophysiologic research into how the human brain reacts to tactile sensations induced by fabrics [74,75]. The cortical responses of the brain to tactile sensations are elicited by skin–fabric interactions, which are characterized by the EEG beta and gamma band activations [76]. Beta oscillations have been shown to be involved in the phasic locking process between the primary and secondary somatosensory cortex in response to tactile sensation [77]. Meanwhile, it was observed that the neuronal assemblies of the sensorimotor cortex were joined in large-scale networks oscillating in the beta band during maintenance of a sustained hand lever press activity [78]. This phenomenon suggested that the primary somatosensory and primary motor cortex were bound together in a beta-synchronized cortical network [78]. Furthermore, Greco et al. found that beta oscillations in the sensorimotor cortex served as an informative feature characterizing affective tactile stimulation by interactions with different fabrics [79]. Singh et al. demonstrated that pleasant and unpleasant tactile sensations present different beta-oscillation patterns [74]. The gamma oscillations of the sensorimotor cortex were also observed in response to tactile sensation. This may reflect the timing code and temporal organization for higher-order somatosensory processing, which is important

for sensory binding [80,81]. In addition, the study by Aya et al. showed that gamma oscillations were simultaneously evoked in the primary and secondary somatosensory cortex during sensory stimulations, thus suggesting that it is critical for forming functional cortico-cortical connections and for conveying somatosensory information from the primary and secondary somatosensory cortex [82]. Bauer et al. found that tactile-stimuli-induced gamma oscillations in the somatosensory cortex were enhanced and prolonged by spatial tactile attention [83]. This indicated that gamma-band synchronization was instrumental in the somatosensory system for processing behaviorally relevant stimulations [83]. Therefore, the RSP variations in the beta and gamma bands were sensitive input features for the SVM-ML model for both unimpaired and stroke persons.

### 3.2. K-Fold Cross Validation

During determination of  $k$  in CV, the model attained the highest accuracy with six-fold CV in the gamma band (Table 3). This was also observed in terms of approximately identical accuracies of the different numbers of  $k$  in the gamma band, which indicated that the SVM-ML model achieved stable classification performance with good generalization capacity for different combinations of training and testing datasets owing to the different  $k$ -fold CV strategies [84]. Furthermore, the model with the leave-one-out CV achieved an accuracy similar to the  $k$ -fold CV technique in the gamma band. This demonstrated the model's unbiased evaluation capability as a special case of  $k$ -fold CV, in which each sample has a chance to represent the entire test dataset [85]. However, the computational cost of the leave-one-out CV was greater than those of other configurations of  $k$  in the  $k$ -fold CV when evaluating the SVM-ML model performance. This was in line with previous studies [85,86] that investigated the computational efficiencies of  $k$ -fold and leave-one-out CV. Thus, it was preferable to use the optimal  $k$ -fold CV, i.e., six-fold CV during model evaluations.

## 4. Generalization of the SVM-ML Model

### 4.1. Different Fabric Stimulations

In the evaluation of model generalization, the wool and nylon fabrics in the gamma band achieved significantly higher accuracies than that of cotton fabric (Table 4 and Figure 5). This was attributable to the differences in their stimulation intensities on the skin. According to the study by Chen et al., neural oscillations in higher frequency bands, e.g., gamma band, were lower when executing an easy task; however, they increased to higher levels to obtain more information from the sensory environment when the task was difficult [87]. Cotton is the most familiar fabric that is in direct contact with skin in daily life, and it provides the lowest stimulation intensity during passive involuntary touch [28]. However, wool and nylon offer more stimulating sensory experiences because of their textile physical properties, which may require additional neural effort and cortical resources to evoke cortical responses to stimulations [28]. This was further supported by the study by Jiao et al., who found that wool elicited a relatively intense tactile stimulation in the form of scratching, resulting in the sensation of discomfort [88]. They also discovered that touching wool fabric elicited higher EEG RSP responses than cotton and nylon fabrics [88]. Hoefer et al. also observed that nylon induced significant higher event-related potential (ERP) signals than cotton, implying that there was less distraction and better cortical resources during tactile sensation [76]. As a result, the model achieved relatively higher accuracies with the RSP features of nylon and wool compared to cotton.

### 4.2. Different Upper-Limb Groups

When considering arm differences, the model yields various patterns for the comparison of accuracies between stimulations with different fabrics (Table 5 and Figure 6). It was observed that the significant differences in the accuracies for classifying post-stroke stimulations with different fabrics shifted to higher frequency bands, i.e., the beta and gamma bands, compared to the UD group. This pattern difference in the classification of stimulations with different fabrics among the different upper-limb groups was similar to

that for manual investigations comparing the EEG RSP differences between stroke and unimpaired persons. In the manual evaluations, the post-stroke representative power spectra to fine touch stimulation shifted to higher frequency bands, i.e., the beta and gamma bands [28]. The sensitivity of the EEG-based RSP features and their capability for feature mapping by the RBF kernel allowed the SVM-ML model to detect similar pattern as manual evaluations. As the input features of the model, the average and maximal values of the RSPs represent the significant differences in RSPs among multiple upper-limb groups. The differences in the EEG RSP patterns in response to fabric stimulations have been discovered in previous manual investigations and were mainly related to neuroplastic changes after stroke [89]. For example, when the damage to the brain neurons result in post-stroke sensorimotor function deficiencies, the cortex composed of various neural subsets could be rewired [90,91]. Neural compensation to lesional functions can lead to redistributed patterns of the cortical responses to external stimulations [92]. Meanwhile, the SVM with RBF kernel can find the optimal decision boundary among multiple upper-limb groups owing to its sufficient feature mapping capability. It implicitly transforms the original RSP features to a high-dimensional feature space with fewer hyperparameters to be determined, which guarantees the generalization capability of the model when supplying new input data [37]. Previous studies have also demonstrated that the SVM with RBF kernel achieves minimal classification error rates in different clinical scenarios while controlling the complexity of the model [36,93,94]. Therefore, based on the sensitivity of the RSP features and the feature mapping capability of the RBF kernel, the proposed model was expected to achieve similar performance as in manual inspection for distinguishing between unimpaired and post-stroke persons.

## 5. Conclusions

In this study, an EEG-based SVM-ML model was established using the RSP features of the EEG signals, i.e.,  $RSP_{\text{mean}}$  and  $RSP_{\text{max}}$ , during stimulation with cotton fabric as the baseline input. The observations demonstrated that the  $RSP_{\text{mean}}$  and  $RSP_{\text{max}}$  were sensitive to fabric stimulations and could be used as representative input features to the model. The generalization performance of the model was investigated by comparing the classification accuracies during stimulations with different fabrics while considering arm differences. The model determined that the significant differences in the accuracies of fabric stimulations after stroke were shifted toward higher bands, i.e., beta and gamma bands, similar to the differences in RSP patterns between post-stroke persons and unimpaired participants as in manual investigations, thereby implying that the model could imitate manual evaluations of cortical responses to fabric stimulations; this ability is expected to aid in automatic assessments of post-stroke fine tactile sensation.

**Author Contributions:** Conceptualization, J.Z. and X.H.; methodology, J.Z. and X.H.; software, J.Z.; validation, Z.L. and J.Z.; data curation, J.Z. and Y.H.; writing—original draft preparation, J.Z.; writing—review and editing, J.Z., Y.H., F.Y., B.Y. and X.H.; supervision, X.H.; funding acquisition, X.H. All authors have read and agreed to the published version of the manuscript.

**Funding:** This research was funded by the National Natural Science Foundation of China, China (NSFC 81771959), the University Grants Committee Research Grants Council, Hong Kong (GRF 15207120), and the Science and Technology Innovation Committee of Shenzhen, China (2021Szvup142).

**Institutional Review Board Statement:** The human experiments were conducted after we obtained the ethical approval from the Human Subjects Ethics Sub-Committee of the Hong Kong Polytechnic University.

**Informed Consent Statement:** Informed consent was obtained from all subjects involved in the study.

**Data Availability Statement:** Data are available upon request.

**Acknowledgments:** The authors would like to thank the participants who participated in this study.

**Conflicts of Interest:** The authors declare no conflict of interest.

## References

1. Kessner, S.S.; Bingel, U.; Thomalla, G. Somatosensory deficits after stroke: A scoping review. *Top. Stroke Rehabil.* **2016**, *23*, 136–146. [[CrossRef](#)] [[PubMed](#)]
2. Sherwood, L. *Human Physiology: From Cells to Systems*; Cengage Learning: Boston, MA, USA, 2015.
3. Carey, L.M.; Matyas, T.A.; Baum, C. Effects of somatosensory impairment on participation after stroke. *Am. J. Occup. Ther.* **2018**, *72*, 7203205100p1–7203205100p10. [[CrossRef](#)] [[PubMed](#)]
4. Tyson, S.F.; Crow, J.L.; Connell, L.; Winward, C.; Hillier, S. Sensory impairments of the lower limb after stroke: A pooled analysis of individual patient data. *Top. Stroke Rehabil.* **2013**, *20*, 441–449. [[CrossRef](#)] [[PubMed](#)]
5. Carey, L.M.; Matyas, T.A.; Oke, L.E. Sensory loss in stroke patients: Effective training of tactile and proprioceptive discrimination. *Arch. Phys. Med. Rehabil.* **1993**, *74*, 602–611. [[CrossRef](#)]
6. Matsuda, K.; Satoh, M.; Tabei, K.-i.; Ueda, Y.; Taniguchi, A.; Matsuura, K.; Asahi, M.; Ii, Y.; Niwa, A.; Tomimoto, H. Impairment of intermediate somatosensory function in corticobasal syndrome. *Sci. Rep.* **2020**, *10*, 11155. [[CrossRef](#)]
7. Cunha, B.P.; Alouche, S.R.; Araujo, I.M.G.; Freitas, S.M.S.F. Individuals with post-stroke hemiparesis are able to use additional sensory information to reduce postural sway. *Neurosci. Lett.* **2012**, *513*, 6–11. [[CrossRef](#)]
8. Boonsinsukh, R.; Panichareon, L.; Phansuwan-Pujito, P. Light touch cue through a cane improves pelvic stability during walking in stroke. *Arch. Phys. Med. Rehabil.* **2009**, *90*, 919–926. [[CrossRef](#)]
9. Johannsen, L.; Wing, A.M.; Hatzitaki, V. Effects of maintaining touch contact on predictive and reactive balance. *J. Neurophysiol.* **2007**, *97*, 2686–2695. [[CrossRef](#)]
10. Campfens, S.F.; Zandvliet, S.B.; Meskers, C.G.; Schouten, A.C.; van Putten, M.J.; van der Kooij, H. Poor motor function is associated with reduced sensory processing after stroke. *Exp. Brain Res.* **2015**, *233*, 1339–1349. [[CrossRef](#)]
11. Doyle, S.D.; Bennett, S.; Dudgeon, B. Upper limb post-stroke sensory impairments: The survivor's experience. *Disabil. Rehabil.* **2014**, *36*, 993–1000. [[CrossRef](#)]
12. Pandyan, A.D.; Johnson, G.R.; Price, C.I.M.; Curless, R.H.; Barnes, M.P.; Rodgers, H. A review of the properties and limitations of the Ashworth and modified Ashworth Scales as measures of spasticity. *Clin. Rehabil.* **1999**, *13*, 373–383. [[CrossRef](#)] [[PubMed](#)]
13. Fugl-Meyer, A.R.; Jääskö, L.; Leyman, I.; Olsson, S.; Stegling, S. The post-stroke hemiplegic patient. 1. a method for evaluation of physical performance. *Scand. J. Rehabil. Med.* **1975**, *7*, 13–31. [[PubMed](#)]
14. Winward, C.E.; Halligan, P.W.; Wade, D.T. The Rivermead Assessment of Somatosensory Performance (RASP): Standardization and reliability data. *Clin. Rehabil.* **2002**, *16*, 523–533. [[CrossRef](#)] [[PubMed](#)]
15. Pan, N. Quantification and evaluation of human tactile sense towards fabrics. *Int. J. Des. Nat. Ecodyn.* **2006**, *1*, 48–60.
16. Auriat, A.M.; Neva, J.L.; Peters, S.; Ferris, J.K.; Boyd, L.A. A Review of Transcranial Magnetic Stimulation and Multimodal Neuroimaging to Characterize Post-Stroke Neuroplasticity. *Front. Neurol.* **2015**, *6*, 226. [[CrossRef](#)]
17. Lundgren, J.; Flodström, K.; Sjögren, K.; Liljequist, B.; Fugl-Meyer, A.R. Site of brain lesion and functional capacity in rehabilitated hemiplegics. *Scand. J. Rehabil. Med.* **1982**, *14*, 141–143.
18. Chollet, F.; DiPiero, V.; Wise, R.J.; Brooks, D.J.; Dolan, R.J.; Frackowiak, R.S. The functional anatomy of motor recovery after stroke in humans: A study with positron emission tomography. *Ann. Neurol.* **1991**, *29*, 63–71. [[CrossRef](#)]
19. Giaquinto, S.; Cobiachi, A.; Macera, F.; Nolfe, G. EEG recordings in the course of recovery from stroke. *Stroke* **1994**, *25*, 2204–2209. [[CrossRef](#)]
20. Broderick, P.A.; Kolodny, E.H. Biosensors for brain trauma and dual laser doppler flowmetry: Enoxaparin simultaneously reduces stroke-induced dopamine and blood flow while enhancing serotonin and blood flow in motor neurons of brain, in vivo. *Sensors* **2010**, *11*, 138–161. [[CrossRef](#)]
21. Radaelli, A.; Mancina, G.; Ferrarese, C.; Beretta, S. *New Concepts in Stroke Diagnosis and Therapy*; Bentham Science Publishers: Milan, Italy, 2017; Volume 1.
22. Chen, Q.; Xia, T.; Zhang, M.; Xia, N.; Liu, J.; Yang, Y. Radiomics in stroke neuroimaging: Techniques, applications, and challenges. *Aging Dis.* **2021**, *12*, 143. [[CrossRef](#)]
23. Militello, C.; Rundo, L.; Dimarco, M.; Orlando, A.; Woitek, R.; D'Angelo, I.; Russo, G.; Bartolotta, T.V. 3D DCE-MRI Radiomic Analysis for Malignant Lesion Prediction in Breast Cancer Patients. *Acad. Radiol.* **2021**, *29*, 830–840. [[CrossRef](#)] [[PubMed](#)]
24. Sharaev, M.; Andreev, A.; Artemov, A.; Burnaev, E.; Kondratyeva, E.; Sushchinskaya, S.; Samotaeva, I.; Gaskin, V.; Bernstein, A. *Pattern Recognition Pipeline for Neuroimaging Data*; Springer: Berlin/Heidelberg, Germany, 2018.
25. Caliandro, P.; Vecchio, F.; Miraglia, F.; Reale, G.; Della Marca, G.; La Torre, G.; Lacidogna, G.; Iacovelli, C.; Padua, L.; Bramanti, P. Small-world characteristics of cortical connectivity changes in acute stroke. *Neurorehabil. Neural Repair* **2017**, *31*, 81–94. [[CrossRef](#)] [[PubMed](#)]
26. Bentes, C.; Peralta, A.R.; Viana, P.; Martins, H.; Morgado, C.; Casimiro, C.; Franco, A.C.; Fonseca, A.C.; Geraldés, R.; Canhão, P. Quantitative EEG and functional outcome following acute ischemic stroke. *Clin. Neurophysiol.* **2018**, *129*, 1680–1687. [[CrossRef](#)] [[PubMed](#)]
27. Ahn, S.-N.; Lee, J.-W.; Hwang, S. Tactile Perception for Stroke Induce Changes in Electroencephalography. *Hong Kong J. Occup. Ther.* **2016**, *28*, 1–6. [[CrossRef](#)] [[PubMed](#)]
28. Huang, Y.; Jiao, J.; Hu, J.; Hsing, C.; Lai, Z.; Yang, Y.; Hu, X.J. Measurement of sensory deficiency in fine touch after stroke during textile fabric stimulation by electroencephalography (EEG). *J. Neural Eng.* **2020**, *17*, 045007. [[CrossRef](#)]

29. Roy, S.; Kiral-Kornek, I.; Harrer, S. ChronoNet: A deep recurrent neural network for abnormal EEG identification. In *Conference on Artificial Intelligence in Medicine in Europe*; Springer: Berlin/Heidelberg, Germany, 2019.
30. Golmohammadi, M.; Ziyabari, S.; Shah, V.; de Diego, S.L.; Obeid, I.; Picone, J. Deep architectures for automated seizure detection in scalp EEGs. *arXiv* **2017**, arXiv:1712.09776.
31. Sirsat, M.S.; Fermé, E.; Câmara, J. Machine Learning for Brain Stroke: A Review. *J. Stroke Cerebrovasc. Dis.* **2020**, *29*, 105162. [[CrossRef](#)]
32. Hosseini, M.-P.; Hemingway, C.; Madamba, J.; McKee, A.; Ploof, N.; Schuman, J.; Voss, E. Review of Machine Learning Algorithms for Brain Stroke Diagnosis and Prognosis by EEG Analysis. *arXiv* **2020**, arXiv:2008.08118.
33. Jochumsen, M.; Rovsing, C.; Rovsing, H.; Niazi, I.K.; Dremstrup, K.; Kamavuako, E.N. Classification of Hand Grasp Kinetics and Types Using Movement-Related Cortical Potentials and EEG Rhythms. *Comput. Intell. Neurosci.* **2017**, *2017*, 7470864. [[CrossRef](#)]
34. Usama, N.; Niazi, I.K.; Dremstrup, K.; Jochumsen, M. Detection of Error-Related Potentials in Stroke Patients from EEG Using an Artificial Neural Network. *Sensors* **2021**, *21*, 6274. [[CrossRef](#)]
35. Iáñez, E.; Azorín, J.M.; Úbeda, A.; Fernández, E.; Sirvent, J.L. LDA-based classifiers for a mental tasks-based brain-computer interface. In Proceedings of the 2010 IEEE International Conference on Systems, Man and Cybernetics, Istanbul, Turkey, 10–13 October 2010.
36. Garrett, D.; Peterson, D.A.; Anderson, C.W.; Thaut, M.H. Comparison of linear, nonlinear, and feature selection methods for EEG signal classification. *IEEE Trans. Neural Syst. Rehabil. Eng.* **2003**, *11*, 141–144. [[CrossRef](#)]
37. Cao, J.; Fang, Z.; Qu, G.; Sun, H.; Zhang, D. An accurate traffic classification model based on support vector machines. *Int. J. Netw. Manag.* **2017**, *27*, e1962. [[CrossRef](#)]
38. Vapnik, V. *The Nature of Statistical Learning Theory*; Springer Science & Business Media: Berlin/Heidelberg, Germany, 2013.
39. Liu, Y.; Zhang, H.; Chen, M.; Zhang, L. A boosting-based spatial-spectral model for stroke patients' EEG analysis in rehabilitation training. *IEEE Trans. Neural Syst. Rehabil. Eng.* **2015**, *24*, 169–179. [[CrossRef](#)]
40. Ghumman, M.K.; Singh, S.; Singh, N.; Jindal, B. Optimization of parameters for improving the performance of EEG-based BCI system. *J. Reliab. Intell. Environ.* **2021**, *7*, 145–156. [[CrossRef](#)]
41. Bousseta, R.; Tayeb, S.; El Ouakouak, I.; Gharbi, M.; Regragui, F.; Himmi, M.M. EEG efficient classification of imagined hand movement using RBF kernel SVM. In Proceedings of the 2016 11th International Conference on Intelligent Systems: Theories and Applications (SITA), Mohammedia, Morocco, 19–20 October 2016.
42. Hsu, C.-W.; Chang, C.-C.; Lin, C.-J. *A Practical Guide to Support Vector Classification*; National Taiwan University: Taipei, Taiwan, 2003.
43. Farid, N.; Elbagoury, B.; Roushdy, M.; Salem, A.-B.M. A comparative analysis for support vector machines for stroke patients. *Recent Adv. Inf. Sci.* **2013**, *41*, 71–76.
44. Kim, M.-K.; Cho, J.-H.; Jeong, J.-H. Classification of Tactile Perception and Attention on Natural Textures from EEG Signals. In Proceedings of the 2021 9th International Winter Conference on Brain-Computer Interface (BCI), Gangwon, Korea, 22–24 February 2021.
45. Lilliefors, H.W. On the Kolmogorov-Smirnov test for the exponential distribution with mean unknown. *J. Am. Stat. Assoc.* **1969**, *64*, 387–389. [[CrossRef](#)]
46. Homan, R.W.; Herman, J.; Purdy, P. Cerebral location of international 10–20 system electrode placement. *Electroencephalogr. Clin. Neurophysiol.* **1987**, *66*, 376–382. [[CrossRef](#)]
47. Welch, P. The use of fast Fourier transform for the estimation of power spectra: A method based on time averaging over short, modified periodograms. *IEEE Trans. Audio Electroacoust.* **1967**, *15*, 70–73. [[CrossRef](#)]
48. Teplan, M. Fundamentals of EEG measurement. *Meas. Sci. Rev.* **2002**, *2*, 1–11.
49. Bronzino, J.D. *Biomedical Engineering Handbook 2*; Springer Science & Business Media: Berlin/Heidelberg, Germany, 2000; Volume 2.
50. Patro, S.; Sahu, K.K. Normalization: A preprocessing stage. *arXiv* **2015**, arXiv:1503.06462. [[CrossRef](#)]
51. Liao, X.; Li, Y.; Hu, J.; Li, Q.; Wu, X. Psychophysical Relations between Interacted Fabric Thermal-Tactile Properties and Psychological Touch Perceptions. *J. Sens. Stud.* **2016**, *31*, 181–192. [[CrossRef](#)]
52. Hu, J.Y.; Hes, L.; Li, Y.; Yeung, K.W.; Yao, B.G. Fabric Touch Tester: Integrated evaluation of thermal–mechanical sensory properties of polymeric materials. *Polym. Test.* **2006**, *25*, 1081–1090. [[CrossRef](#)]
53. Bishop, C.M. *Pattern Recognition and Machine Learning*; Springer: Berlin/Heidelberg, Germany, 2006.
54. Syarif, I.; Prugel-Bennett, A.; Wills, G. SVM parameter optimization using grid search and genetic algorithm to improve classification performance. *Telkommnika* **2016**, *14*, 1502. [[CrossRef](#)]
55. Zhang, Y.; Ji, X.; Liu, B.; Huang, D.; Xie, F.; Zhang, Y. Combined feature extraction method for classification of EEG signals. *Neural Comput. Appl.* **2017**, *28*, 3153–3161. [[CrossRef](#)]
56. Guler, I.; Ubeyli, E.D. Multiclass support vector machines for EEG-signals classification. *IEEE Trans. Inf. Technol. Biomed.* **2007**, *11*, 117–126. [[CrossRef](#)]
57. Avelino, J.; Paulino, T.; Cardoso, C.; Moreno, P.; Bernardino, A. Human-aware natural handshaking using tactile sensors for Vizzy, a social robot. In Proceedings of the Workshop on Behavior Adaptation, Interaction and Learning for Assistive Robotics at RO-MAN, Lisbon, Portugal, 28 August–1 September 2017.
58. Pedregosa, F.; Varoquaux, G.; Gramfort, A.; Michel, V.; Thirion, B.; Grisel, O.; Blondel, M.; Prettenhofer, P.; Weiss, R.; Dubourg, V. Scikit-learn: Machine learning in Python. *J. Mach. Learn. Res.* **2011**, *12*, 2825–2830.

59. Kattenstroth, J.-C.; Kalisch, T.; Peters, S.; Tegenthoff, M.; Dinse, H. Long-term sensory stimulation therapy improves hand function and restores cortical responsiveness in patients with chronic cerebral lesions. Three single case studies. *Front. Hum. Neurosci.* **2012**, *6*, 244. [[CrossRef](#)]
60. Pfurtscheller, G.; Neuper, C. Motor imagery activates primary sensorimotor area in humans. *Neurosci. Lett.* **1997**, *239*, 65–68. [[CrossRef](#)]
61. James, G.; Witten, D.; Hastie, T.; Tibshirani, R. *An Introduction to Statistical Learning*; Springer: Berlin/Heidelberg, Germany, 2013; Volume 112.
62. Breiman, L. Heuristics of instability and stabilization in model selection. *Ann. Stat.* **1996**, *24*, 2350–2383. [[CrossRef](#)]
63. Witten, I.H.; Frank, E. Data mining: Practical machine learning tools and techniques with Java implementations. *Acm Sigmod Rec.* **2002**, *31*, 76–77. [[CrossRef](#)]
64. Bouckaert, R.R. Choosing between two learning algorithms based on calibrated tests. *ICML* **2003**, *3*, 51–58.
65. Kuhn, M.; Johnson, K. *Applied Predictive Modeling*; Springer: Berlin/Heidelberg, Germany, 2013; Volume 26.
66. Chang, M.-W.; Lin, C.-J. Leave-one-out bounds for support vector regression model selection. *Neural Comput.* **2005**, *17*, 1188–1222. [[CrossRef](#)]
67. Burges, C.J.C. A tutorial on support vector machines for pattern recognition. *Data Min. Knowl. Discov.* **1998**, *2*, 121–167. [[CrossRef](#)]
68. Vivaldi, N.; Caiola, M.; Solarana, K.; Ye, M. Evaluating performance of eeg data-driven machine learning for traumatic brain injury classification. *IEEE Trans. Biomed. Eng.* **2021**, *68*, 3205–3216. [[CrossRef](#)]
69. Gao, L.; Cheng, W.; Zhang, J.; Wang, J. EEG classification for motor imagery and resting state in BCI applications using multi-class Adaboost extreme learning machine. *Rev. Sci. Instrum.* **2016**, *87*, 085110. [[CrossRef](#)] [[PubMed](#)]
70. Kira, K.; Rendell, L.A. A practical approach to feature selection. In *Machine Learning Proceedings*; Elsevier: Amsterdam, The Netherlands, 1992; pp. 249–256.
71. Kitada, R.; Hashimoto, T.; Kochiyama, T.; Kito, T.; Okada, T.; Matsumura, M.; Lederman, S.J.; Sadato, N. Tactile estimation of the roughness of gratings yields a graded response in the human brain: An fMRI study. *Neuroimage* **2005**, *25*, 90–100. [[CrossRef](#)]
72. Wu, J.; Srinivasan, R.; Quinlan, E.B.; Solodkin, A.; Small, S.L.; Cramer, T.C. Utility of EEG measures of brain function in patients with acute stroke. *J. Neurophysiol.* **2016**, *115*, 2399–2405. [[CrossRef](#)]
73. Singh, H.; Bauer, M.; Chowanski, W.; Sui, Y.; Atkinson, D.; Baurley, S.; Fry, M.; Evans, J.; Bianchi-Berthouze, N. The brain's response to pleasant touch: An EEG investigation of tactile caressing. *Front. Hum. Neurosci.* **2014**, *8*, 893. [[CrossRef](#)]
74. Merabet, L.B.; Pascual-Leone, A. Neural reorganization following sensory loss: The opportunity of change. *Nat. Rev. Neurosci.* **2010**, *11*, 44–52. [[CrossRef](#)]
75. Ackerley, R.; Carlsson, I.; Wester, H.; Olausson, H.; Backlund Wasling, H. Touch perceptions across skin sites: Differences between sensitivity, direction discrimination and pleasantness. *Front. Behav. Neurosci.* **2014**, *8*, 54. [[CrossRef](#)]
76. Hoefer, D.; Handel, M.; Müller, K.M.; Hammer, T.R. Electroencephalographic study showing that tactile stimulation by fabrics of different qualities elicit graded event-related potentials. *Ski. Res. Technol.* **2016**, *22*, 470–478. [[CrossRef](#)] [[PubMed](#)]
77. Simões, C.; Jensen, O.; Parkkonen, L.; Hari, R. Phase locking between human primary and secondary somatosensory cortices. *Proc. Natl. Acad. Sci. USA* **2003**, *100*, 2691–2694. [[CrossRef](#)] [[PubMed](#)]
78. Brovelli, A.; Ding, M.; Ledberg, A.; Chen, Y.; Nakamura, R.; Bressler, S.L. Beta oscillations in a large-scale sensorimotor cortical network: Directional influences revealed by Granger causality. *Proc. Natl. Acad. Sci. USA* **2004**, *101*, 9849–9854. [[CrossRef](#)] [[PubMed](#)]
79. Greco, A.; Guidi, A.; Bianchi, M.; Lanata, A.; Valenza, G.; Scilingo, E.P. Brain dynamics induced by pleasant/unpleasant tactile stimuli conveyed by different fabrics. *IEEE J. Biomed. Health Inform.* **2019**, *23*, 2417–2427. [[CrossRef](#)] [[PubMed](#)]
80. Hasenstaub, A.; Shu, Y.; Haider, B.; Kraushaar, U.; Duque, A.; McCormick, D.A. Inhibitory postsynaptic potentials carry synchronized frequency information in active cortical networks. *Neuron* **2005**, *47*, 423–435. [[CrossRef](#)]
81. Engel, A.K.; Singer, W. Temporal binding and the neural correlates of sensory awareness. *Trends Cogn. Sci.* **2001**, *5*, 16–25. [[CrossRef](#)]
82. Ihara, A.; Hirata, M.; Yanagihara, K.; Ninomiya, H.; Imai, K.; Ishii, R.; Osaki, Y.; Sakihara, K.; Izumi, H.; Imaoka, H.; et al. Neuromagnetic gamma-band activity in the primary and secondary somatosensory areas. *NeuroReport* **2003**, *14*, 273–277. [[CrossRef](#)] [[PubMed](#)]
83. Bauer, M.; Oostenveld, R.; Peeters, M.; Fries, P. Tactile spatial attention enhances gamma-band activity in somatosensory cortex and reduces low-frequency activity in parieto-occipital areas. *J. Neurosci.* **2006**, *26*, 490–501. [[CrossRef](#)]
84. Xiong, Z.; Cui, Y.; Liu, Z.; Zhao, Y.; Hu, M.; Hu, J. Evaluating explorative prediction power of machine learning algorithms for materials discovery using k-fold forward cross-validation. *Comput. Mater. Sci.* **2020**, *171*, 109203. [[CrossRef](#)]
85. Refaeilzadeh, P.; Tang, L.; Liu, H. Cross-validation. *Encycl. Database Syst.* **2009**, *5*, 532–538.
86. Jung, Y. Multiple predicting K-fold cross-validation for model selection. *J. Nonparametr. Stat.* **2018**, *30*, 197–215. [[CrossRef](#)]
87. Chen, A.; Wang, A.; Wang, T.; Tang, X.; Zhang, M. Behavioral oscillations in visual attention modulated by task difficulty. *Front. Psychol.* **2017**, *8*, 1630. [[CrossRef](#)] [[PubMed](#)]
88. Jiao, J.; Hu, X.; Huang, Y.; Hu, J.; Hsing, C.; Lai, Z.; Wong, C.; Xin, J.H. Neuro-perceptive discrimination on fabric tactile stimulation by Electroencephalographic (EEG) spectra. *PLoS ONE* **2020**, *15*, e0241378. [[CrossRef](#)] [[PubMed](#)]
89. Snyder, D.B.; Schmit, B.D.; Hyngstrom, A.S.; Beardsley, S.A. Electroencephalography resting-state networks in people with Stroke. *Brain Behav.* **2021**, *11*, e02097. [[CrossRef](#)]

90. Dąbrowski, J.; Czajka, A.; Zielińska-Turek, J.; Jaroszyński, J.; Furtak-Niczyporuk, M.; Mela, A.; Poniatowski, Ł.A.; Drop, B.; Dorobek, M.; Barcikowska-Kotowicz, M. Brain functional reserve in the context of neuroplasticity after stroke. *Neural Plast.* **2019**, *2019*, 9708905. [[CrossRef](#)]
91. Voss, P.; Thomas, M.E.; Cisneros-Franco, J.M.; de Villers-Sidani, É. Dynamic brains and the changing rules of neuroplasticity: Implications for learning and recovery. *Front. Psychol.* **2017**, *8*, 1657. [[CrossRef](#)]
92. Lin, M.P.; Liebeskind, D.S. Imaging of ischemic stroke. *Contin. Lifelong Learn. Neurol.* **2016**, *22*, 1399. [[CrossRef](#)]
93. Sun, S.; Zhang, C. Adaptive feature extraction for EEG signal classification. *Med. Biol. Eng. Comput.* **2006**, *44*, 931–935. [[CrossRef](#)]
94. Al-Qazzaz, N.K.; Ali, S.H.B.M.; Ahmad, S.A.; Islam, M.S.; Escudero, J. Discrimination of stroke-related mild cognitive impairment and vascular dementia using EEG signal analysis. *Med. Biol. Eng. Comput.* **2018**, *56*, 137–157. [[CrossRef](#)]